World Scientific
www.worldscientific.com

Optical penetration of surface-enhanced micro-scale spatial offset Raman spectroscopy in turbid gel and biological tissue

Yumin Zhang*, Li Lin*, Jing He* and Jian Ye*,†,‡

*School of Biomedical Engineering
Shanghai Jiao Tong University
Shanghai, P. R. China

†Shanghai Key Laboratory of Gynecologic Oncology
Ren Ji Hospital, School of Medicine
Shanghai Jiao Tong University
Shanghai, P. R. China
‡yejian78@sjtu.edu.cn

The limited penetration of photons in biological tissue restricts the deep-tissue detection and imaging application. The micro-scale spatially offset Raman spectroscopy (micro-SORS) with an optical fiber probe, colleting photons from deeper regions by offsetting the position of laser excitation from the collection optics in a range of hundreds of microns, shows great potential to be integrated with endoscopy for inside-body noninvasive detection by circumventing this restriction, particularly with the combination of surface-enhanced Raman spectroscopy (SERS). However, a detailed tissue penetration study of micro-SORS in combination with SERS is still lacking. Herein, we compared the signal decay of enhanced Raman nanotags through the tissue phantom of agarose gel and the biological tissue of porcine muscle in the near-infrared (NIR) region using a portable Raman spectrometer with a micro-SORS probe (2.1 mm in diameter) and a conventional hand-held probe (9.7 mm in diameter). Two kinds of Raman nanotags were prepared from gold nanorods decorated with the nonresonant (4-nitrobenzenethiol) or resonant Raman reporter molecules (IR-780 iodide). The SERS measurements show that the penetration depths of two Raman nanotags are both over 2 cm in agarose gel and 3 mm in porcine muscle. The depth could be improved to over 4 cm in agarose gel and 5 mm in porcine tissue when using the micro-SORS system. This demonstrates the superiority of optical-fiber micro-SORS system over the conventional Raman detection for the detection of nanotags in deeper layers in the turbid medium and biological tissue, offering the possibility of combining the micro-SORS technique with SERS for noninvasive *in vivo* endoscopy-integrated clinical application.

Yumin Zhang and Li Lin contributed equally to this work.
‡Corresponding author.

1. Introduction

Despite the advances of *in-vivo* spectroscopy-based biomedical imaging at the near-infrared (NIR) biological window in the fields of medicine, life science and clinical applications, the limited penetration of photons in biological tissues still restricts the deep-tissue detection and bioimaging application.[1–3] Due to the nature of high diffusion and scattering of photons in tissues, the loss of signal and the yield of noise are hardly evitable. For instance, a penetration depth of only a few millimeters is reported for fluorescence imaging at the NIR window.[1,4] Therefore, the optical fiber-based endoscopy shows great potential for a clinical inside-body detection. Endoscopes have been developed for many parts of the body, inserted through the tubular organs including lung, colon, stomach, uterus, etc.[5–8] Compared to the large imaging modalities such as computed tomography (CT) or magnetic resonance imaging (MRI), the endoscopy techniques are more effective in the diagnostics of small lesions or lesions in tubular organs during a surgery. By using endoscopy, the spectroscopic signals only need to penetrate the tube wall and/or a layer of tissues. The requirement of photon penetration depth could thus be shortened to millimeters to several centimeters, largely benefiting the *in-vivo* detection and bioimaging applications.

Raman spectroscopy that provides information of molecular composition and structure in a non-destructive way is a promising optical method for bioimaging and detection.[9,10] However, the conventional Raman measurements using the microscope or the hand-held probe only allow limited depth sensing at the NIR window with a depth ranging from hundreds of micrometers to a few millimeters.[11] In the recent decade, the deep Raman techniques have been developed to greatly improve the penetration depth of Raman detection, by collecting diffuse Raman photons from an area of the subsurface.[12] One of these techniques is the spatially offset Raman spectroscopy (SORS), which collects photons from deeper subsurface regions by offsetting the point of laser excitation from the collection optics.[13,14] This utilizes the concept that photons emerging from deeper layers in turbid media have to traverse larger distances via diffuse migration. Traditional SORS usually has a spatial offset of millimeters or more, and the reported largest penetration depth of SORS reached 5 cm.[15] The SORS with a small spatial offset of hundreds of microns has also been developed, named as micro-scale spatially offset Raman spectroscopy (micro-SORS).[16] The micro-SORS is usually combined with Raman microscopic objective, designed to resolve the thin and highly turbid layers such as stratified polymers, painted sculptures, paper and wheat seeds.[16–19] Full micro-SORS, which includes fully separated laser illumination and Raman collection areas but the dimensions of the two zones on sample surface remain constant, possesses the highest performance and largest penetration depth compared with the other variants of micro-SORS.[16,20] However, it is difficult to focus the laser beam on a spot nearby the Raman collection spot particularly when high magnification microscopic objectives with a short working distance are used. Therefore, the method of optical fibers combined with full micro-SORS technique exhibits huge advantages.[21] In this method, two separated fibers are used, one for optical excitation and the other for collection. This allows to utilize a small laser spot and collect the Raman signal at a relatively short distance of spatial offset without limitations. More importantly, it is possible to use the fiber-based micro-SORS in endoscopy-integrated *in-vivo* applications where a hand-held probe or a microscopic objective would not be applicable. Therefore, micro-SORS technique is considered to not only show better penetration performance than conventional Raman probes, but have the advantages of endoscopic probes in detecting small lesions inside the body, promising for *in-vivo* biomedical imaging and detections.

Surface-enhanced Raman spectroscopy (SERS) is an ultrasensitive vibrational spectroscopic technique based on the plasmon-enhanced local electric fields near the surfaces of nanostructures.[22–25] With plasmonic substrates such as gold (Au) or silver (Ag) nanoparticles (NPs) for the adsorption of

specific Raman reporter molecules, SERS can reach an enhancement factor as high as 10^{10}–10^{11}, enabling the detection of a single molecule with the highly specific, noninvasive monitoring of the chemical composition.[26–28] When using a Raman reporter molecule with an electronic transition close to the incident laser frequency, several orders of magnitude enhancement in SERS signal can be further obtained, which is the surface-enhanced resonance Raman spectroscopy (SERRS).[29–31] The combination of SERS and SORS generates the technique of surface-enhanced spatially offset Raman spectroscopy (SESORS), achieving the sensing capability at larger depths. Using SORS with millimeters of spatial offset, SERS signals were detectable up to 6.75 mm of the porcine tissue and 8 mm of bone.[32,33] Additionally, by adopting the resonance SESORS technique, i.e., SESORRS, Nicolson *et al.* successfully detected signals up to 25 mm of the porcine tissue, and the 3D live breast cancer tumor models up to 15 mm of the tissue.[34] In the other relevant studies where the incident and collection beams are on the opposite side (namely, the transmission Raman), bisphosphonates in bone have been detected *ex vivo* first through a 20-mm-thick specimen of porcine muscle tissue and Stone and co-workers successfully detected SERS NPs embedded in a porcine tissue at the depths of up to 5 cm.[15,35] These techniques have largely improved the penetration depth of Raman detection, opening the way for the noninvasive monitoring of deep layers in live tissues, e.g., the *in-vivo* glucose sensing and through-skull detection of neurochemicals.[36,37]

Nevertheless, although SESORS (or SESORRS) technique has been reported in the literature, most of the studies used the conventional SORS with spatial offset in millimeters, instead of the micro-SORS with spatial offset in microns. The detailed fundamental studies of micro-SORS in combination with SERS (or SERRS) are still lacking. Moreover, it is of practical significance to investigate the performance of micro-SORS with an integrated fiber-bundle probe, considering the potential in further clinical applications. By comparing the SERS nanotag signals collected from commercial Raman spectrometer with a normal hand-held probe and that with a micro-SORS probe, it is possible to evaluate the penetration depth of Raman spectroscopy in different media, such as biological tissues or turbid gels. In addition, the comparison of photons propagating in the turbid medium between SERS

and SERRS nanotags by using micro-SORS may provide more insights on the penetration limit induced by the differences in signal intensities. These data could be valuable references for further *in-vivo* applications of Raman spectroscopy.

In this work, we have investigated the penetration performance using the portable NIR Raman spectrometer with either a conventional hand-held backscattering probe or an integrated fiber-bundle micro-SORS probe by using SERS and SERRS nanotags [Fig. 1(a)]. Au nanorods (NRs) were used as the SERS substrate due to their tunable plasmon resonance effect in the NIR biological window. Raman nanotags were prepared by modifying the plasmonic Au NRs with the nonresonant Raman reporter molecules [4-nitrobenzenethiol (4-NBT)] and the resonant reporters (IR-780 iodide). These SERS and SERRS nanotags exhibit pronounced and characteristic Raman spectra under the excitation of 785-nm laser, both reaching the detection limit as low as 2 pM. Detailed comparisons of Raman signals and the penetration depth measurement of these nanotags in the agarose gels and biological tissues using two Raman probe configurations were also performed, showing better performance of fiber-bundle-based micro-SORS technique and demonstrating the superiority of SESORRS for monitoring in deeper layers in the turbid medium. We have also studied the variations in penetration depth for SERS or SERRS nanotags induced by their different signal intensities. Our work provides valuable information toward the application of micro-SORS technique for *in-vivo* measurements in the clinically relevant circumstances.

2. The Main Text

2.1. *Materials and methods*

2.1.1. *Materials*

All chemicals were obtained commercially and used as-received without any further purification. Cetyltrimethylammonium bromide (CTAB; $\geq 99\%$), sodium borohydride (NaBH$_4$; 98%) and sulfuric acid (H$_2$SO$_4$; 98%) were obtained from J&K Chemical Ltd. (Shanghai, China). Chloroauric acid tetrahydrate (HAuCl$_4 \cdot$ 4H$_2$O) was purchased from Sinopharm Chemical Reagent Co., Ltd. (Shanghai, China). Silver nitrate (AgNO$_3$; 99.8%), ascorbic acid (AA; $> 99\%$) and agarose (for biochemistry)

were purchased from Aladdin (China). Also, 4-NBT was obtained from Fluorochem Ltd. (UK). IR-780 iodide ($\geq 95\%$) was purchased from Sigma-Aldrich (China). Ultrapure water obtained from Milli-Q Integral 5 system was used in all the experiments.

2.1.2. *Synthesis of SERS and SERRS nanotags*

Au NRs were first prepared by a seed-mediated growth method.[38] First, 0.3 mL of 10-mM $NaBH_4$ in ice water was added to 5-mL aqueous solution containing 2.5 mL of 0.5-mM $HAuCl_4$ and 2.5 mL of 0.2-M CTAB under vigorous stirring. Then, the seed solution was incubated in a water bath at 30°C for 2 h. The growth solution was obtained by mixing 100 mL of 0.1-M CTAB, 1 mL of 10-mM $AgNO_3$, 5 mL of 10-mM $HAuCl_4$, 0.8 mL of 0.1-M AA and 2 mL of 0.512-M H_2SO_4. After mixing the growth solution for 30 min, 250 μL of the seed solution was added under vigorous stirring, and then the solution was incubated in 30°C water bath for 12 h in the dark. The product was washed with water two times and was redispersed in 20 mL of water.

NR@4-NBT SERS nanotags were prepared as follows. 1 mL of the prepared Au NRs was mixed with 3 mL of water, and 100 μL of 10-mM 4-NBT in ethanol was added under vigorous sonication. The mixture was incubated at 30°C for 30 min. Then the product was washed with 10-mM CTAB two times and finally redispersed in 1 mL of 10-mM CTAB.

NR@IR-780 SERRS nanotags were prepared as follows. First, 1 mL of the prepared Au NRs was mixed with 3 mL of water, and 100 μL of 0.16-mM IR-780 in *N,N*-dimethylformamide was added under vigorous sonication.[39,40] The mixture was then incubated at 30°C for 1 h. Finally, the product was washed with water two times and the supernatant was removed. The precipitates were redispersed in 1 mL of water.

2.1.3. *Calculation of NPs concentration*

To calculate the concentration of NPs, each Au NR was considered as a cylinder with two spherical ends, a length (l) of 56 nm and a width (d) of 14 nm [determined by transmission electron microscopy (TEM)]. Thus, the volume of this particle is $V = \pi(l-d)(d/2)^2 + (\pi d^3)/6 \approx 7902\,\mathrm{nm}^3$. The mass of one NR is $m = \rho V = 1.53 \times 10^{-16}$ g. The total mass of Au for synthesizing Au NRs is

9.85×10^{-3} g, and hence the concentration of Au NRs is $9.85 \times 10^{-3}/(1.53 \times 10^{-16} \times 6.02 \times 10^{23} \times 0.02) = 5.34$ nM. Then the NPs were diluted to the range of 0.2–200 pM when collecting the SERS spectra via confocal Raman microscope.

2.1.4. *Characterization of SERS and SERRS nanotags*

The ultraviolet–visible (UV–Vis) absorbance spectra were measured with a UV1900 UV–Vis Spectrometer (Aucybest, China). TEM images of the nanomaterials were acquired with a JME-2100F transmission electron microscope (JEOL, Japan) operating at 200 kV. Raman measurements of aqueous SERS and SERRS nanotags were performed on a confocal Raman microscope (XploRA INV, Horiba) using 785-nm (29.8-mW laser power, 1-s integration time) and 532-nm (45-mW laser power, 5-s integration time) irradiations through a 10 × objective lens (NA = 0.3).

2.1.5. *Raman penetration depth measurement*

To measure the penetration depth of Raman signals, the agarose gel was utilized. Agarose aqueous solution (0.5 wt.%) was heated in microwave oven until the turbid solution became clear. Agarose solution was quickly added into SERS or SERRS nanotags under vigorous sonication, and then 1 mL of the solution was transferred to a well container with a final concentration of 0.3 nM. The mixture cooled down to room temperature in 30 min, and the solid agarose gel containing SERS or SERRS nanotags (named as Raman tag gel) was taken out and put on silicon wafer.

Pure agarose gel (without nanotags) was obtained in a similar way. Pure agarose gel of 0–8-cm thickness was placed on the top of Raman tag gel for the Raman penetration depth measurements. The penetration depth measurement on porcine muscle was performed in a similar manner by just replacing the pure agarose gel with porcine muscle. The penetration depth measurement of Raman signal was performed with a hand-held Raman spectrometer (SEED 3000-R2, OCEANHOOD, 200-mW 785-nm laser) and a home-built integrated SORS system (Andor Ivac-316 CCD, EMvision HT-SPEC-785-01-IVAC spectrograph, EMvision HT-PROB-ENDO-785 Raman probe, 10-mW 785-nm laser). The working distance and spot diameter of hand-held probe are about 7.5 mm and 150 μm,

respectively. The spatial offset probe consists of seven fibers arranged in a 2.1-mm-diameter circle with the diameter of each fiber being $300\,\mu$m and 500-μm working distance.

2.1.6. *Data analysis*

The spectra collected in the penetration measurement were first processed by the baseline correction with adaptive iteratively reweighted Penalized Least Squares (airPLS) method to remove the fluorescence background. Then the Raman intensity was calculated as the difference between the maximum value of the Raman peak ($1208\,\mathrm{cm}^{-1}$ for NR@IR-780 and $1332\,\mathrm{cm}^{-1}$ for NR@4-NBT) and baseline. The Raman intensities in the above Raman shift of the blank sample, i.e., the pure agarose gel or porcine muscle, were considered as the background noise. The detection threshold was calculated as three times the standard deviation of the noise. The penetration depth was determined by maximum thickness of the turbid medium with which on top the Raman signal of SERS tag gel was still detectable.

2.1.7. *FDTD simulations*

The extinction cross-section and electric field enhancement distributions of the Au NR were simulated by employing the finite-difference time-domain (FDTD) method with the commercial software FDTD Solutions (Lumerical, Inc.). Dielectric permittivity of Au was from empirical data and was further fitted with Lumerical's multi-coefficient model (MCM).[41] The surrounding medium in the simulating region was set as water with a refractive index of 1.33. An additional region covering the whole nanostructure with a refined mesh of 0.5 nm was utilized to improve the structural resolution of the Au NR. The wavelength range of the excitation source was set from $200\,$nm to $1100\,$nm. Longitudinal and transversal excitations with perpendicular polarizations were performed in three individual simulations and the final extinction cross-section was processed by weighted averaging the results from these simulations.

2.2. *Results and discussion*

The schematic illustrations of a Raman penetration depth measurement with (i) a micro-SORS fiber-bundle probe and (ii) a conventional backscattering probe are shown in Fig. 1(a). First, the Raman tag gel containing SERS nanotags in a disk shape was placed on a silicon wafer. The wafer serves here as a substrate to enhance the collection of Raman signals. Then the pure agarose gel with a thickness d is
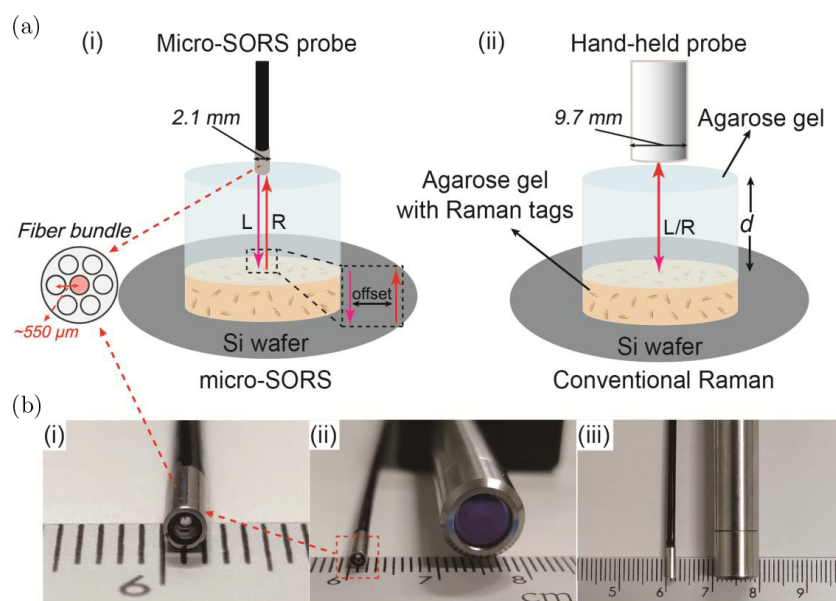

Fig. 1. (Color online) (a) Schematic illustration of Raman penetration depth (d) measurement with (i) micro-SORS with an integrated fiber-bundle probe and (ii) conventional backscattering Raman spectroscopy with a hand-held probe. The micro-SORS probe consists of seven optical fibers with the center one (red) for the excitation and the other six for the collection. Legend: L: incident light, R: Raman light. (b) Photos of (i), (ii) the cross-section and (iii) side views of (left) micro-SORS probe and (right) hand-held probe.

carefully placed on the top of a Raman tag gel, ensuring no air bubble in between. Finally, a Raman spectrometer with a spatial offset or conventional hand-held probe is utilized to excite and collect Raman signals of Raman tag gel from the top. In fact, a successful Raman penetration measurement includes two steps: (1) penetration of incident light by a distance of d to excite the Raman nanotags; and (2) the passing of consequent Raman scattered light through a distance of d again to be collected. The penetration depth is obtained by continuously increasing the thickness of agarose gel to reach the maximum value until the Raman signal is undetectable. In our experiments, the Raman signal of pure agarose gel or porcine muscle was considered as the background noise. The detection threshold was calculated as three times the standard deviation of the noise. The Raman penetration measurement in biological tissue was performed in a similar manner by only replacing the agarose gel with porcine muscle. Figure 1(b) shows the experimental Raman probes: panels (i) and (ii) show the cross-section and panel (iii) shows the side views of the probes. The micro-SORS probe is composed of an optical fiber bundle with an external diameter of 2.1 mm, which is suitable to be inserted into the working channel of a conventional endoscope. The fiber bundle consists of seven fibers with each one being 300 μm in diameter and the middle one is used as excitation fiber and the others are for collection. It can be calculated that the micro-scale spatial offset (micro-Δs), i.e., the distance between the centers of excitation and collection fibers, in such a small probe is about 550 μm. The diameter of the hand-held probe is 9.7 mm, much larger (about five times) than that of the micro-SORS one.

The SERS and SERRS nanotags used in this work were obtained using the Au NRs as the enhancement substrate due to their highly tunable plasmon resonance in the NIR region. The Au NRs capped with CTAB surfactant molecules were first prepared by a seed-mediated growth method reported before [Fig. 2(a)(i)]. To obtain Au NRs-based Raman tags, the NRs were functionalized with a self-assembled molecular layer of Raman reporter molecules, either via the Au–S covalent bonding for 4-NBT [Fig. 2(a)(ii)] or through the electrostatic adsorption and hydrophobic effect for IR-780 iodide molecules [Fig. 2(a)(iii)].[42] TEM characterization shows that Au NRs are uniform

with the average sizes of 56 nm in length and 14 nm in width [Fig. 2(d)(i)] and keep the particle morphology unchanged after the modification by 4-NBT or IR-780 iodide molecules [Figs. 2(d)(ii) and 2(d)(iii)]. Figure 2(b) illustrates the optical properties of Au NRs and those after modification with the nonresonant molecule 4-NBT and resonant reporter IR-780 iodide. Au NRs show a slightly broadened longitudinal plasmon resonance at $\sim$ 820 nm [curve i in Fig. 2(b)], which is exactly overlapping with the 785-nm laser and the absorption wavelength of IR-780 iodide (780 nm) for obtaining the SERS and SERRS tags.[31,43] After being modified with 4-NBT molecules, the increase in refractive index surrounding the NPs results in a red shift and the broadening of the longitudinal plasmon resonance [curve ii in Fig. 2(b)]. The broadening of the resonance may be partially contributed by the slight NR aggregation during the preparation process. More interestingly, we find that the decoration of NRs with IR-780 iodide molecules leads to a blue shift of the dipolar longitudinal plasmon resonance of NRs from 826 nm to 801 nm, which is most likely due to the removal of CTAB molecules during the decoration process [curve iii in Fig. 2(b)]. A slightly broadened resonance with an extra peak appears at 879 nm probably caused by the slight aggregation of NRs. These mild aggregation of NRs after being functionalized with IR-780 iodide would not affect the subsequent study in this work. FDTD simulations have been additionally performed to better understand the plasmonic behaviors of the Au NR. The calculated far-field extinction spectrum of an Au NR (56 nm in length and 14 nm in width) shows a dipolar longitudinal plasmon resonance at 815 nm and a transverse plasmon resonance at 515 nm [curve iv in Fig. 2(b)], which fits well with experimental results. The corresponding strong electromagnetic field enhancement distribution at 785 nm demonstrates that NR is a quite suitable plasmonic substrate for constructing the SERS and SERRS tags in the NIR region [Fig. 2(c)]. The much weaker electromagnetic enhancement confirms the off-resonance condition at 532 nm for the NR. The schematic preparation process and the corresponding photographs of Raman tag gels are shown in Figs. 2(e) and 2(f), respectively. Briefly, 0.5-wt.% agarose solution with a temperature of over 70°C was quickly injected to the aqueous Raman tag (Au NR@4-NBT or Au NR@IR-780) solution under
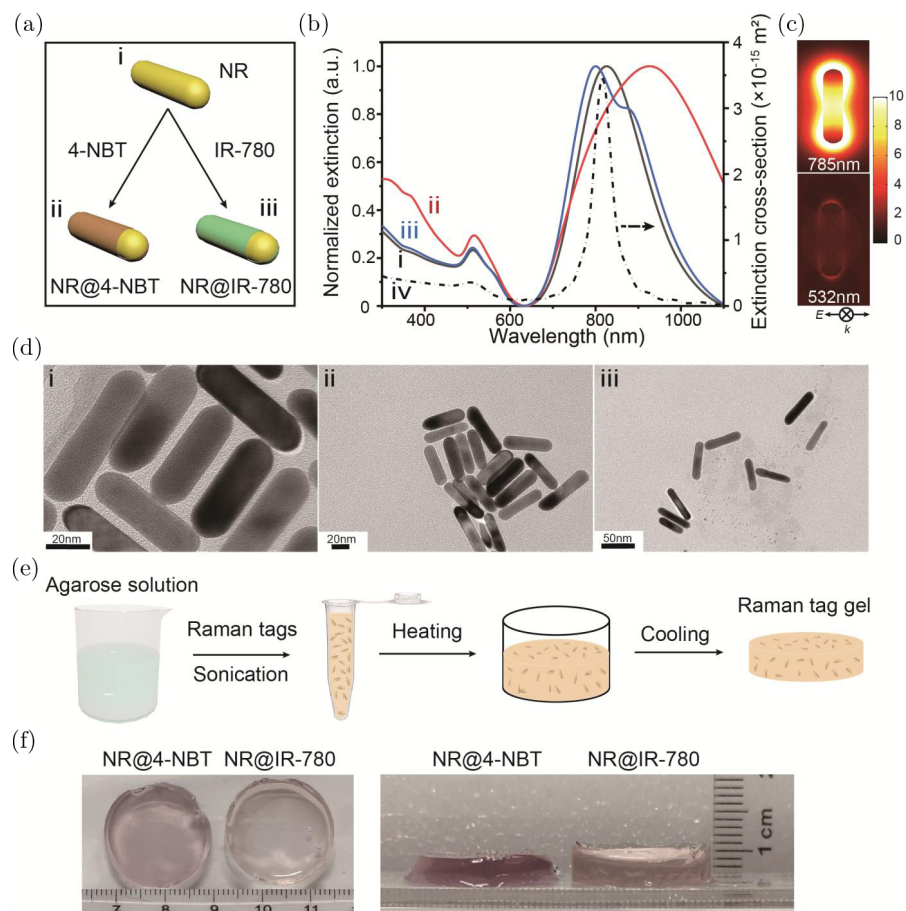
Fig. 2. (a) Schematic illustration of the synthesis of Au NR-based Raman nanotags. (b) Experimental extinction spectra of Au NRs (curve i), NR@4-NBT (curve ii), NR@IR-780 (curve iii) and FDTD simulated extinction spectrum of an Au NR (56 nm in length and 14 nm in width; curve iv). All experimental extinction spectra are normalized. (c) The FDTD-calculated electric field enhancement distributions of Au NR at the wavelengths of 785 nm and 532 nm. The incident light propagation (k) and polarization direction (E) are indicated below the photographs. (d) TEM images of (i) Au NRs, (ii) NR@4-NBT and (iii) NR@IR-780. (e) The scheme of preparation procedure and (f) photographs of agarose gel with Raman nanotags (NR@4-NBT or NR@IR-780).

vigorous sonication. This process would not affect the SERS and SERRS nanotags since the nanotags can still maintain good dispersion after a 70°C water bath.[44] Subsequently, the mixture was added into a well container and kept at room temperature for 30 min. After the clotting of agarose molecules, the Raman tag gel was formed as a three-dimensional matrix of about 2.4 cm in diameter and about 0.4 cm in thickness. In this way, we are able to obtain a Raman signal source in a nonliquid state while maintaining the good dispersity of NPs as much as possible.

Next, we investigated the Raman performance of aqueous SERS nanotags (NR@4-NBT) and SERRS nanotags (NR@IR-780) under the resonant (785-nm) and off-resonant (532-nm) excitation conditions. The Raman spectrum of SERS tags (NR@4-NBT) of 200 pM shows pronounced Raman bands at 1085, 1332 and 1570 cm^{-1} at 785-nm excitation, which correspond to the in-plane C–H bending vibration, nitro group and the C–C ring stretching mode [Fig. 3(a)].[45] By considering the excitation laser power and integration time (29.8 mW and 1 s for 785 nm; 45 mW and 5 s for 532 nm), NR@4-NBT exhibits the Raman intensity with roughly one order of magnitude smaller at 532 nm [Fig. 3(b)]. Further examination of their concentration-dependent Raman spectra discloses that the detection limit of NR@4-NBT, determined by the intensity of 1332-cm^{-1} band, can reach as low as 2 pM and 20 pM for 785-nm and 532-nm excitations, respectively [Figs. 3 (a)–3(c)]. Similarly, we measured the Raman spectra of SERRS colloidal (NR@IR-780) solution under 785-nm and 532-nm excitations [Figs. 3(d) and 3(e)],
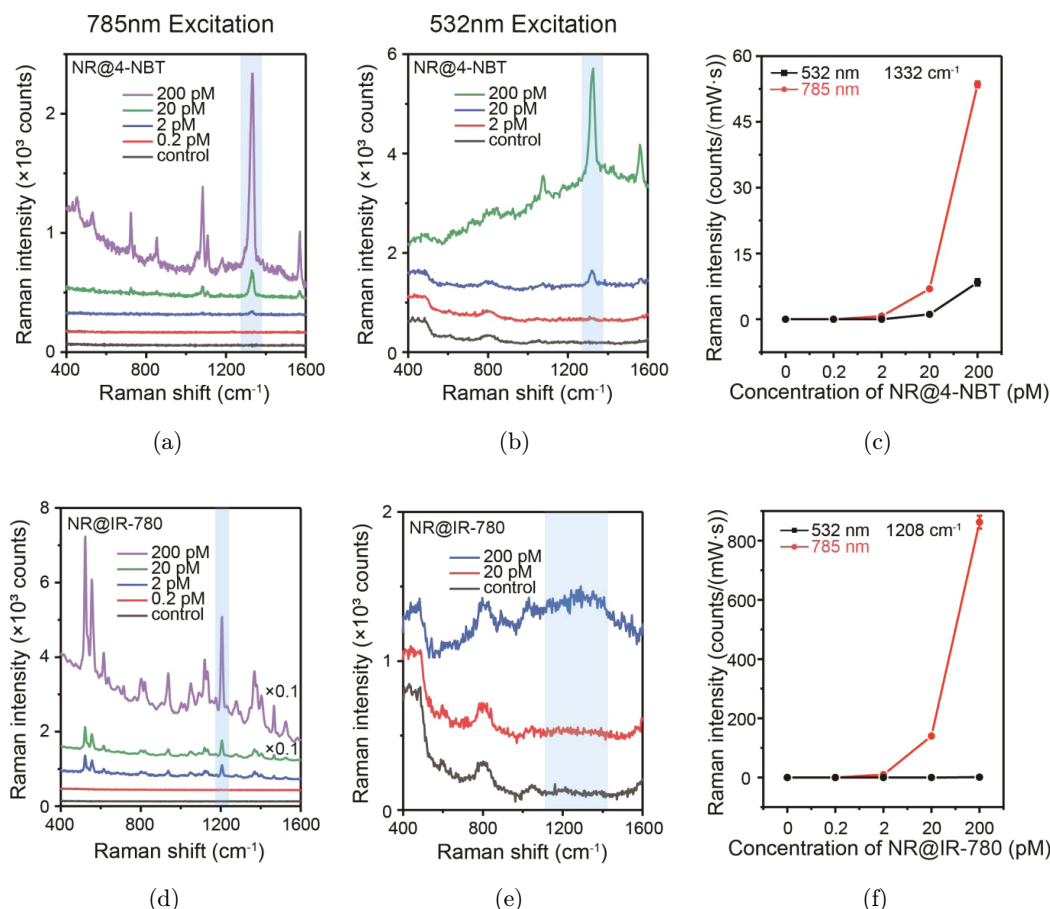
Fig. 3. (Color online) Limit of detection of aqueous Raman nanotags. (a), (b) Concentration-dependent SERS spectra of NR@4-NBT and (c) the Raman intensity [1332-cm^{-1} band, indicated by the blue area in panels (a) and (b)] plot excited by 785-nm and 532-nm laser. (d), (e) Concentration-dependent SERS spectra of NR@IR-780 and (f) the Raman intensity [1208-cm^{-1} band, indicated by the blue area in panels (d) and (e)] plot excited by 785-nm and 532-nm laser. The laser powers of 532 nm and 785 nm are 45 mW and 29.8 mW, respectively.

and only the former provokes the pronounced Raman bands of 941, 1208, 1371 and 1465 cm^{-1}, corresponding to the vibration modes of C–C bending, C–C stretching, –CH$_2$– twisting and –CH$_2$– scissoring.[46] The intensity of the Raman band at 1208 cm^{-1} is used here to determine the detection limit of NR@IR-780. The results in Fig. 3(f) shows that the detection limit of NR@IR-780 SERRS nanotags can reach 2 pM and 200 pM for 785-nm and 532-nm excitations, respectively. All above measurements were repeatedly performed three times and the error bars represent the standard deviations. It can be found that these Raman nanotags (including SERS and SERRS nanotags) exhibit much stronger Raman signals under 785-nm excitation compared to that of 532-nm one. This could be well explained by the enhanced electric field of Au NRs at 785 nm, as predicted by the FDTD simulations

[Fig. 2(c)]. IR-780 iodide, a commercial fluorescent dye with an absorption peak at around 780 nm, serves herein as a resonant Raman reporter molecule. The huge difference in intensities of NR@IR-780 under two wavelength lasers further proved the resonance effect of IR-780 molecule at around 785 nm. In addition, it is worth noting that the Raman intensity of 200-pM NR@IR-780 colloids is roughly one order of magnitude higher than that of 200-pM NR@4-NBT, which could be owing to the resonance Raman effect of IR-780 iodide. However, both Raman nanotags exhibit the same detection limit (2 pM) under 785-nm excitation. We assume that this is due to the not so enough sensitivity of Raman spectrometer system with the current measurement condition, i.e., the intensity differences between two NPs not being distinguishable any more.

Quantitative measurements on the depth-dependent Raman signal decay were performed using the turbid phantom consisting of agarose gels since they have tissue-like scattering properties.[47] The concentration of agarose gel reported for mimic tissue analogs covers the range of 0.5–7 wt.%.[48–53] In this work, our main purpose is to study the difference between conventional backscattering Raman spectroscopy and micro-SORS under the same condition, so the concentrations of agarose gel does not affect our results. We chose 0.5-wt.% agarose solution to prepare the Raman gel as a demonstration of the tissue analogs. The agarose gel with nanotags was used to mimic solid tumor with

NPs. The Raman spectra of SERS (NR@4-NBT) and SERRS nanotags (NR@IR-780) were collected with different thicknesses of agarose gel from 0 cm to 8 cm using a 785-nm Raman spectrometer with a micro-SORS probe [Figs. 4(a)–4(c)]. Different integration times were used for SERS [0.5 s, Fig. 4(b)] and SERRS nanotags [0.05 s, Fig. 4(c)] due to the different SERS performances. The Raman intensity per second versus the thickness of gel was plotted on the right of each panel. The pure agarose gel was used as the control group for the confirmation of detectable Raman signals. The specific Raman mode ($1332 \, cm^{-1}$ for 4-NBT, and $1208 \, cm^{-1}$ for IR-780) was used to define the penetration depth in
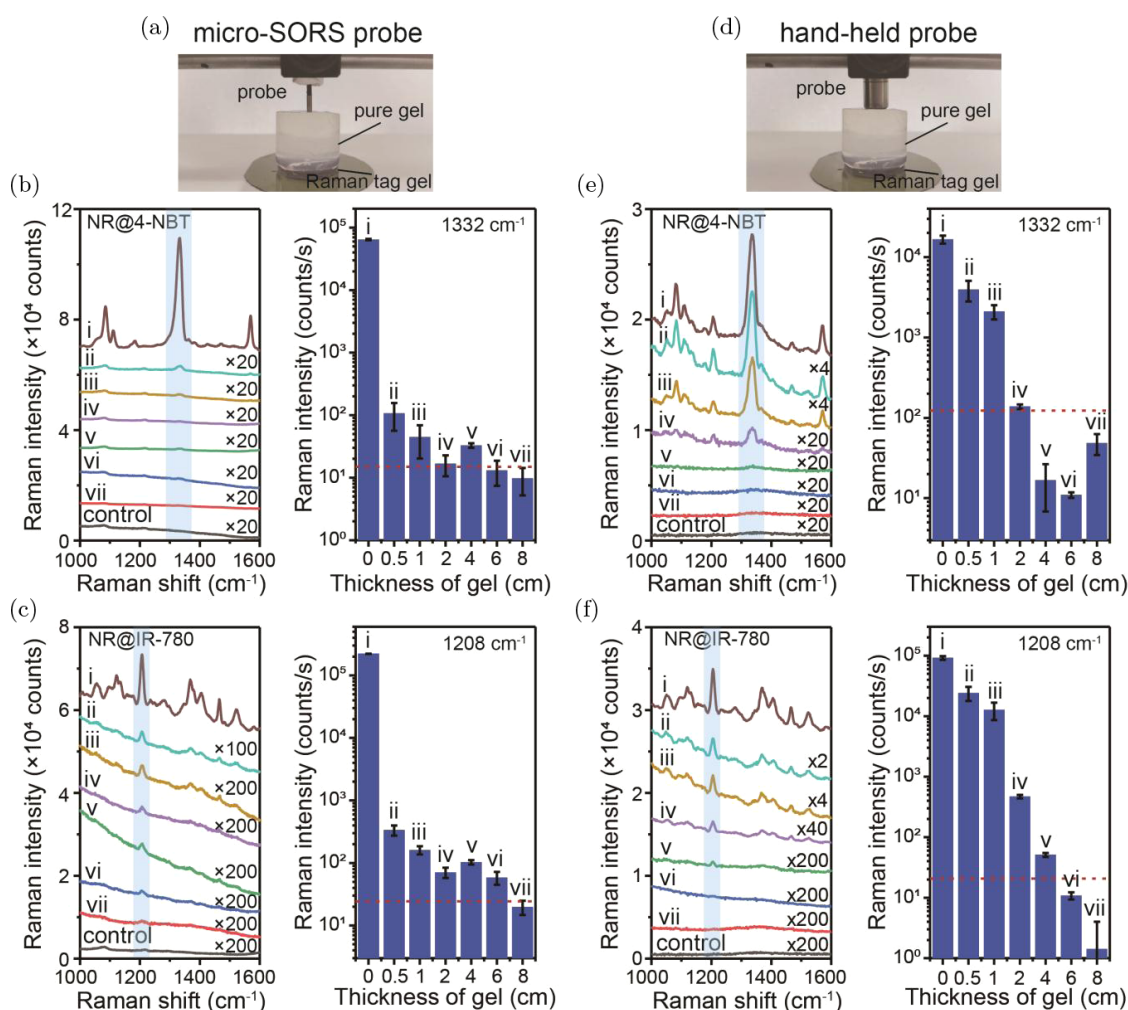

Fig. 4. (Color online) Raman penetration depth measurements on agarose gel of different thicknesses: (i) 0 cm, (ii) 0.5 cm, (iii) 1 cm, (iv) 2 cm, (v) 4 cm, (vi) 6 cm and (vii) 8 cm. Control sample is pure agarose gel. (a) The setup collecting Raman spectra with the micro-SORS probe and the corresponding collected Raman spectra on (b) NR@4-NBT gel and (c) NR@IR-780 gel. (d) The setup collecting Raman spectra with a conventional hand-held probe and the corresponding Raman spectra on (e) NR@4-NBT gel and (f) NR@IR-780 gel. The histograms on the right of panels (b), (c), (e) and (f) show the Raman intensities per second of the 1332-cm^{-1} and 1208-cm^{-1} bands and the red dashed line indicates the detection threshold.

turbid agarose gel. The plots of Raman intensities versus the gel thickness show that the Raman intensity of the pure Raman tag gel could be beyond 10^3 counts per mW $\cdot$ s. It has been noted that the decay percentage of Raman intensity is impressively over 99% when 0.5-cm-thick gel was placed on the Raman tag gel. The Raman intensity gradually further decreases with the increase of gel thickness and finally to a value less than the threshold (red dashed line), the Raman peak is dominant by random noise when its intensity is lower than the detection threshold. In this case, the penetration depths of NR@4-NBT and NR@IR-780 on agarose gel could be more than 4 cm and 6 cm, respectively,

when using a 785-nm Raman spectrometer with a micro-SORS probe. This indicates that the brighter Raman nanotags are more likely to be detected in the deeper layers, which induces the differences in penetration depth of the two Raman tag gels. This can be understood by the fact that more photons can reach the detection surface and be detected by the collection probe. Figures 4(d)–4(f) show the Raman spectra of NR@4-NBT and NR@IR-780 nanotags with different thicknesses of agarose gel on them, collected using a 785-nm Raman spectrometer with a hand-held probe. Raman peaks in the spectra of v–vii in Fig. 4(e) and vi and vii in Fig. 4(f) are below the detection threshold (red dashed lines).
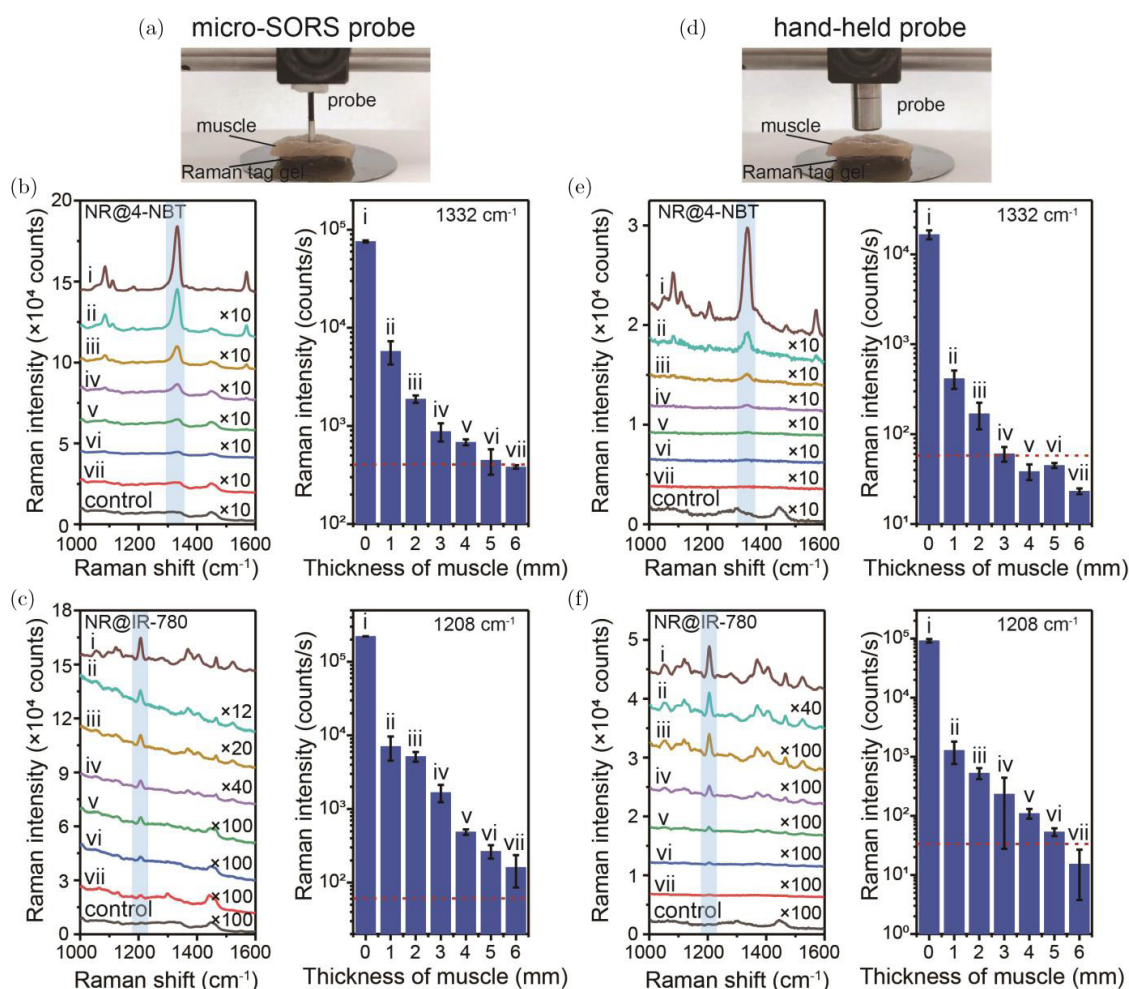

Fig. 5. Raman penetration depth measurements on porcine muscle of different thicknesses: (i) 0 mm, (ii) 1 mm, (iii) 2 mm, (iv) 3 mm, (v) 4 mm, (vi) 5 mm and (vii) 6 mm. (a) The setup collecting Raman spectra with the micro-SORS probe and the corresponding collected Raman spectra on (b) NR@4-NBT gel and (c) NR@IR-780 gel. (d) The setup collecting Raman spectra with a conventional hand-held probe and the corresponding Raman spectra on (e) NR@4-NBT gel and (f) NR@IR-780 gel. The histograms on the right of panels (b), (c), (e) and (f) show the Raman intensities per second of the 1332-cm^{-1} and 1208-cm^{-1} bands and the red dashed line indicates the detection threshold.

Therefore, these peaks are more like random noises and their intensities no longer obey the attenuation distribution when 4–8-cm and 6–8-cm pure gels were put on the top of Raman tag gel, respectively. Careful analysis of Raman signal decay indicates that the penetration depths of NR@4-NBT and NR@IR-780 on agarose gels could be over 2 cm and 4 cm, respectively [Figs. 4(e) and 4(f)]. It is worth noting that when 0.5 cm of phantom gel was placed on the top, the Raman intensity decreases by $\sim 80\%$. We also noticed the different decay rates between micro-SORS probe system and hand-held probe system when 0.5 and 1 cm of phantom gels were placed on the top. This is most likely due to the different working distances of these two kinds of probes. But interestingly, the penetration depth measured using Raman spectrometer with a micro-SORS probe is deeper than that using a hand-held probe for both kinds of nanotags, which demonstrates the better performance of micro-SORS probe in gaining signal from the deeper layers of agarose gel. These results show that a much deeper penetration can be achieved when using a Raman spectrometer with the micro-SORS probe compared to the one with the hand-held probe, confirming the superiority of micro-SORS in combination with SERRS for the monitoring in deeper layers of the turbid medium.

We then expanded the investigation of Raman penetration depth measurements on biological tissues. Figures 5(a) and 5(d) show that the Raman signals were measured using porcine muscle as the penetration medium and a similar experimental setup was used for the agarose gel. The Raman spectra of NR@4-NBT and NR@IR-780 with different thicknesses of porcine muscle from 0 mm to 6 mm on the top were collected using a 785-nm Raman spectrometer with the micro-SORS probe [Figs. 5(b) and 5(c)]. The integration time of the spectra is 0.5 s for NR@4-NBT nanotags [Fig. 5(b)] and 0.05 s for NR@IR-780 nanotags [Fig. 5(c)]. The pure muscle tissue was used as the control group. The Raman intensities per second of 1332-cm^{-1} and 1208-cm^{-1} bands are plotted on the right of each panel to determine the Raman penetration depth in porcine muscle. It can be found that the Raman intensity greatly drops by over 96% when 1-mm muscle was placed on the top, owing to the high scattering of photons in the biological tissues. The Raman intensity further continuously decreases with the increase of muscle tissue thickness and the

penetration depths of NR@4-NBT and NR@IR-780 tags in porcine muscle are determined to be about 5 mm and 6 mm [Figs. 5(b) and 5(c)], respectively. Figures 5(e) and 5(f) show the corresponding Raman signal decays of two kinds of tags in different thicknesses of porcine muscle, collected by a Raman spectrometer with the hand-held probe. The Raman intensity greatly drops by over 98% when 1-mm muscle was placed on the top, this decay rate is slightly faster than that when using a micro-SORS probe. The final penetration depths of NR@4-NBT and NR@IR-780 from the above evaluation are determined to be 3 mm and 5 mm in the porcine muscle under 785-nm excitation with the hand-held probe, respectively. This shows the advantages of the micro-SORS in gaining better signal from deep layers of muscle tissues.

2.3. *Conclusions*

In this work, we investigated the optical penetration performance of the Raman spectrometer with an integrated micro-SORS probe and a conventional hand-held probe using SERS (or SERRS) in the NIR region. Two kinds of Raman nanotags were prepared from plasmonic Au NRs decorated with the nonresonant (4-NBT) and resonant Raman reporter (IR-780 iodide) molecules, serving as the ideal NIR SERS and SERRS tags with utilization of the strong electromagnetic enhancement of the longitudinal dipolar mode of Au NRs. The concentration-dependent Raman measurements show that the detection limits of two kinds of nanotags can both reach as low as 2 pM. It can be also noticed that NR@IR-780 exhibits one order of magnitude stronger Raman signal than NR@4-NBT due to the resonance Raman effect. Further detailed thickness-dependent measurements show that the Raman penetration depth is over 2 cm in agarose gel and 3 mm in porcine muscle for NR@4-NBT, and is over 4 cm in agarose gel and 5 mm in porcine muscle for NR@IR-780, when using a NIR Raman spectrometer with a conventional hand-held probe. The penetration depth can reach larger than 4 cm and 6 cm for NR@4-NBT and NR@IR-780 nanotags in agarose gel, respectively, when using a NIR spectrometer with the micro-SORS probe. The micro-SORS system also improves the penetration depth in porcine muscle up to 5 cm and 6 mm for NR@4-NBT and NR@IR-780 nanotags, respectively. These results demonstrate the superiority of the

Y. Zhang et al.

fiber-based micro-SORS technique for the Raman detection in deeper layers in the turbid medium and porcine tissue. This work represents a significant step forward in the detection of Raman signals located in depth *in vivo* where the conventional Raman detection is not able to arrive at due to a high level of diffuse scattering and millimeter-scale SORS would not be applicable due to the large size of the setup and the probe. It offers new possibility of combining the optical-fiber micro-SORS technique with SERS (or SERRS) for noninvasive endoscopy-based clinical applications.

Conflicts of Interest

There are no conflicts of interest relevant to this article.

Acknowledgments

References

1. G. Hong, A. L. Antaris, H. Dai, "Near-infrared fluorophores for biomedical imaging," *Nat. Biomed. Eng.* **1**, 0010 (2017).
2. Z. Bao, Y. Zhang, Z. Tan, X. Yin, W. Di, J. Ye, "Gap-enhanced Raman tags for high-contrast sentinel lymph node imaging," *Biomaterials* **163**, 105–115 (2018).
3. S. Raimondo, G. Zito, "Imaging to study solid tumour origin and progression: Lessons from research and clinical oncology," *Immunol. Cell Biol.* **95**, 531–537 (2017).
4. K. Welsher, S. P. Sherlock, H. J. Dai, "Deep-tissue anatomical imaging of mice using carbon nanotube fluorophores in the second near-infrared window," *Proc. Natl. Acad. Sci. USA* **108**, 8943–8948 (2011).
5. J. Liu, Q. Y. Lin, K. Blazek, B. H. Liang, X. M. Guan, "Transvaginal natural orifice transluminal endoscopic surgery myomectomy: A novel route for uterine myoma removal," *J. Minim. Invasive Gynecol.* **25**, 959–960 (2018).
6. T. Itoi, T. H. Baron, M. A. Khashab, T. Tsuchiya, S. Irani, V. Dhir, A. Y. B. Teoh, "Technical review of endoscopic ultrasonography-guided gastroenterostomy in 2017," *Dig. Endosc.* **29**, 495–502 (2017).
7. I. Skovgaard Christiansen, J. C. Kuijvenhoven, U. Bodtger, T. M. H. Naur, K. Ahmad, J. Singh Sidhu, R. Nessar, G. N. Salih, A. Hoegholm, J. T. Annema, P. F. Clementsen, "Endoscopic ultrasound with bronchoscope-guided fine needle aspiration for the diagnosis of paraesophageally located lung lesions," *Respiration* **97**, 277–283 (2019).
8. W. Marlicz, K. Skonieczna-Zydecka, D. E. Yung, I. Loniewski, A. Koulaouzidis, "Endoscopic findings and colonic perforation in microscopic colitis: A systematic review," *Dig. Liver Dis.* **49**, 1073–1085 (2017).
9. E. Cordero, I. Latka, C. Matthaus, I. W. Schie, J. Popp, "*In-vivo* Raman spectroscopy: From basics to applications," *J. Biomed. Opt.* **23**, 071210 (2018).
10. Y. Zhou, C. H. Liu, Y. Pu, B. L. Wu, T. A. Nguyen, G. G. Cheng, L. X. Zhou, K. Zhu, J. Chen, Q. B. Li, R. R. Alfano, "Combined spatial frequency spectroscopy analysis with visible resonance Raman for optical biopsy of human brain metastases of lung cancers," *J. Innov. Opt. Health Sci.* **12**, 1950010 (2019).
11. L. A. Lane, R. Y. Xue, S. M. Nie, "Emergence of two near-infrared windows for *in vivo* and intraoperative SERS," *Curr. Opin. Chem. Biol.* **45**, 95–103 (2018).
12. P. Matousek, N. Stone, "Development of deep subsurface Raman spectroscopy for medical diagnosis and disease monitoring," *Chem. Soc. Rev.* **45**, 1794–1802 (2016).
13. P. Matousek, M. D. Morris, N. Everall, I. P. Clark, M. Towrie, E. Draper, A. Goodship, A. W. Parker, "Numerical simulations of subsurface probing in diffusely scattering media using spatially offset Raman spectroscopy," *Appl. Spectrosc.* **59**, 1485–1492 (2005).
14. P. Matousek, I. P. Clark, E. R. C. Draper, M. D. Morris, A. E. Goodship, N. Everall, M. Towrie, W. F. Finney, A. W. Parker, "Subsurface probing in diffusely scattering media using spatially offset Raman spectroscopy," *Appl. Spectrosc.* **59**, 393–400 (2005).
15. N. Stone, M. Kerssens, G. R. Lloyd, K. Faulds, D. Graham, P. Matousek, "Surface enhanced spatially offset Raman spectroscopic (SESORS) imaging — the next dimension," *Chem. Sci.* **2**, 776–780 (2011).
16. C. Conti, M. Realini, C. Colombo, P. Matousek, "Comparison of key modalities of micro-scale

spatially offset Raman spectroscopy," *Analyst* **140**, 8127–8133 (2015).

17. C. Conti, C. Colombo, M. Realini, G. Zerbi, P. Matousek, "Subsurface Raman analysis of thin painted layers," *Appl. Spectrosc.* **68**, 686–691 (2014).

18. C. Conti, C. Colombo, M. Realini, P. Matousek, "Subsurface analysis of painted sculptures and plasters using micrometre-scale spatially offset Raman spectroscopy (micro-SORS)," *J. Raman Spectrosc.* **46**, 476–482 (2015).

19. C. Conti, M. Realini, C. Colombo, K. Sowoidnich, N. K. Afseth, M. Bertasa, A. Botteon, P. Matousek, "Noninvasive analysis of thin turbid layers using microscale spatially offset Raman spectroscopy," *Anal. Chem.* **87**, 5810–5815 (2015).

20. M. Realini, C. Conti, A. Botteon, C. Colombo, P. Matousek, "Development of a full micro-scale spatially offset Raman spectroscopy prototype as a portable analytical tool," *Analyst* **142**, 351–355 (2017).

21. P. Vandenabeele, C. Conti, A. Rousaki, L. Moens, M. Realini, P. Matousek, "Development of a fiber-optics microspatially offset Raman spectroscopy sensor for probing layered materials," *Anal. Chem.* **89**, 9218–9223 (2017).

22. L. Lin, Q. Zhang, X. Y. Li, M. Qiu, X. Jiang, W. Jin, H. C. Gu, D. Y. Lei, J. Ye, "Electron transport across plasmonic molecular nanogaps interrogated with surface-enhanced Raman scattering," *ACS Nano* **12**, 6492–6503 (2018).

23. P. L. Stiles, J. A. Dieringer, N. C. Shah, R. R. Van Duyne, "Surface-enhanced Raman spectroscopy," *Annu. Rev. Anal. Chem.* **1**, 601–626 (2008).

24. J. M. Nam, J. W. Oh, H. Lee, Y. D. Suh, "Plasmonic nanogap-enhanced Raman scattering with nanoparticles," *Acc. Chem. Res.* **49**, 2746–2755 (2016).

25. L. Lin, H. C. Gu, J. Ye, "Plasmonic multi-shell nanomatryoshka particles as highly tunable SERS tags with built-in reporters," *Chem. Commun.* **51**, 17740–17743 (2015).

26. W. E. Doering, S. M. Nie, "Single-molecule and single-nanoparticle SERS: Examining the roles of surface active sites and chemical enhancement," *J. Phys. Chem. B* **106**, 311–317 (2002).

27. S. M. Nie, S. R. Emery, "Probing single molecules and single nanoparticles by surface-enhanced Raman scattering," *Science* **275**, 1102–1106 (1997).

28. N. G. Khlebtsov, L. Lin, B. N. Khlebtsov, J. Ye, "Gap-enhanced Raman tags: Fabrication, optical properties, and theranostic applications," *Theranostics* **10**, 2067–2094 (2020).

29. D. Graham, K. Faulds, "Quantitative SERRS for DNA sequence analysis," *Chem. Soc. Rev.* **37**, 1042–1051 (2008).

30. A. Mallinger, K. Schiemann, C. Rink, F. Stieber, M. Calderini, S. Crumpler, M. Stubbs, O. Adeniji-Popoola, O. Poeschke, M. Busch, P. Czodrowski, D. Musil, D. Schwarz, M. J. Ortiz-Ruiz, R. Schneider, C. Thai, M. Valenti, A. de Haven Brandon, R. Burke, P. Workman, T. Dale, D. Wienke, P. A. Clarke, C. Esdar, F. I. Raynaud, S. A. Eccles, F. Rohdich, J. Blagg, "Discovery of potent, selective, and orally bioavailable small-molecule modulators of the mediator complex-associated kinases CDK8 and CDK19," *J. Med. Chem.* **59**, 1078–1101 (2016).

31. H. K. Yuan, Y. Liu, A. M. Fales, Y. L. Li, J. Liu, T. Vo-Dinh, "Quantitative surface-enhanced resonant Raman scattering multiplexing of biocompatible gold nanostars for *in vitro* and *ex vivo* detection," *Anal. Chem.* **85**, 208–212 (2013).

32. S. M. Asiala, N. C. Shand, K. Faulds, D. Graham, "Surface-enhanced, spatially offset Raman spectroscopy (SESORS) in tissue analogues," *ACS Appl. Mater. Interfaces* **9**, 25488–25494 (2017).

33. B. Sharma, K. Ma, M. R. Glucksberg, R. P. Van Duyne, "Seeing through Bone with surface-enhanced spatially offset Raman spectroscopy," *J. Am. Chem. Soc.* **135**, 17290–17293 (2013).

34. F. Nicolson, L. E. Jamieson, S. Mabbott, K. Plakas, N. C. Shand, M. R. Detty, D. Graham, K. Faulds, "Through tissue imaging of a live breast cancer tumour model using handheld surface enhanced spatially offset resonance Raman spectroscopy (SESORRS)," *Chem. Sci.* **9**, 3788–3792 (2018).

35. H. N. Xie, R. Stevenson, N. Stone, A. Hernandez-Santana, K. Faulds, D. Graham, "Tracking bisphosphonates through a 20 mm thick porcine tissue by using surface-enhanced spatially offset Raman spectroscopy," *Angew. Chem., Int. Ed.* **51**, 8509–8511 (2012).

36. J. M. Yuen, N. C. Shah, J. T. Walsh, M. R. Glucksberg, R. P. Van Duyne, "Transcutaneous glucose sensing by surface-enhanced spatially offset Raman spectroscopy in a rat model," *Anal. Chem.* **82**, 8382–8385 (2010).

37. A. S. Moody, P. C. Baghernejad, K. R. Webb, B. Sharma, "Surface enhanced spatially offset Raman spectroscopy detection of neurochemicals through the skull," *Anal. Chem.* **89**, 5689–5693 (2017).

38. N. Zhao, Z. R. Yang, B. X. Li, J. Meng, Z. L. Shi, P. Li, S. Fu, "RGD-conjugated mesoporous silica-encapsulated gold nanorods enhance the sensitization of triple-negative breast cancer to megavoltage radiation therapy," *Int. J. Nanomed.* **11**, 5595–5610 (2016).

39. X. Y. Bi, Y. Q. Gu, J. Ye, "Ag-coated Au nanopetals: Dual-type single-nanoparticle detection of

gap-enhanced resonance Raman tags," *ACS Appl. Nano Mater.* **3**, 6987–6995 (2020).

40. Y. Q. Gu, X. Y. Bi, J. Ye, "Gap-enhanced resonance Raman tags for live-cell imaging," *J. Mater. Chem. B* **8**, 6944–6955 (2020).

41. P. B. Johnson, R. W. Christy, "Optical constants of the noble metals," *Phys. Rev. B* **6**, 4370–4379 (1972).

42. Y. Q. Zhang, Y. Q. Gu, J. He, B. D. Thackray, J. Ye, "Ultrabright gap-enhanced Raman tags for high-speed bioimaging," *Nat. Commun.* **10**, 3905 (2019).

43. T. Nagy-Simon, M. Potara, A. M. Craciun, E. Licarete, S. Astilean, "IR780-dye loaded gold nanoparticles as new near infrared activatable nanotheranostic agents for simultaneous photodynamic and photothermal therapy and intracellular tracking by surface enhanced resonant Raman scattering imaging," *J. Colloid Interface Sci.* **517**, 239–250 (2018).

44. X. L. Jin, B. N. Khlebtsov, V. A. Khanadeev, N. G. Khlebtsov, J. Ye, "Rational design of ultrabright SERS probes with embedded reporters for bioimaging and photothermal therapy," *ACS Appl. Mater. Interfaces* **9**, 30387–30397 (2017).

45. K. Kim, J. Y. Choi, K. S. Shin, "Surface-enhanced Raman scattering of 4-nitrobenzenethiol and 4-aminobenzenethiol on silver in icy environments at liquid nitrogen temperature," *J. Phys. Chem. C* **118**, 11397–11403 (2014).

46. Y. X. Guo, Z. F. Zhuang, Z. M. Liu, W. D. Fan, H. Q. Zhong, W. Zhang, Y. R. Ni, Z. Y. Guo, "Facile hot spots assembly on molybdenum oxide nanosheets via *in situ* decoration with gold nanoparticles," *Appl. Surf. Sci.* **480**, 1162–1170 (2019).

47. M. Balu, T. Baldacchini, J. Carter, T. B. Krasieva, R. Zadoyan, B. J. Tromberg, "Effect of excitation wavelength on penetration depth in nonlinear optical microscopy of turbid media," *J. Biomed. Opt.* **14**, 010508 (2009).

48. Y. R. Lee, S. Lee, D. G. Kim, "Enhancement of emulsion penetration in agarose gel model using flexible plasma treatment," *Biomed. Phys. Eng. Express* **5**, 045027 (2019).

49. A. J. Wright, S. P. Poland, J. M. Girkin, C. W. Freudiger, C. L. Evans, X. S. Xie, "Adaptive optics for enhanced signal in CARS microscopy," *Opt. Express* **15**, 18209–18219 (2007).

50. D. Dobrynin, G. Fridman, G. Friedman, A. A. Fridman, "Deep penetration into tissues of reactive oxygen species generated in floating electrode dielectric barrier discharge (FE-DBD): An *in vitro* agarose gel model mimicking an open wound," *Plasma Med.* **2**, 71–83 (2012).

51. T. R. Kwon, J. Seok, J. H. Jang, M. K. Kwon, C. T. Oh, E. J. Choi, H. K. Hong, Y. S. Choi, J. Bae, B. J. Kim, "Needle-free jet injection of hyaluronic acid improves skin remodeling in a mouse model," *Eur. J. Pharm. Biopharm.* **105**, 69–74 (2016).

52. H. Wang, T. B. Huff, Y. Fu, K. Y. Jia, J.-X. Cheng, "Increasing the imaging depth of coherent anti-Stokes Raman scattering microscopy with a miniature microscope objective," *Opt. Lett.* **32**, 2212–2214 (2007).

53. D. W. Zhang, D. B. Das, C. D. Rielly, "Microneedle assisted micro-particle delivery from gene guns: Experiments using skin-mimicking agarose gel," *J. Pharm. Sci.* **103**, 613–627 (2014).